Fabrication of $NiFe_2O_4/SiO_2/TiO_2$ Magnetic Composite for Effective Photodegradation of Congo Red Dye

Poedji Loekitowati Hariani[1,2*], Salni Salni[3], Melviana Violetta Kimur[1], Nurlisa Hidayati[1], and Elfita Elfita[1]

[1]*Department of Chemistry, Faculty of Mathematics and Natural Sciences, Universitas Sriwijaya, Jl. Palembang Prabumulih Km. 32, Ogan Ilir 30662, Indonesia*

[2]*Research Group on Magnetic Materials, Department of Chemistry, Faculty of Mathematics and Natural Sciences, Universitas Sriwijaya, Jl. Palembang Prabumulih Km. 32, Ogan Ilir 30662, Indonesia*

[3]*Department of Biology, Faculty of Mathematics and Natural Sciences, Universitas Sriwijaya, Jl. Palembang Prabumulih Km. 32, Ogan Ilir 30662, Indonesia*

* ***Corresponding author:***

email: puji_lukitowati@mipa.unsri.ac.id

Received: February 17, 2024
Accepted: March 25, 2025

DOI: 10.22146/ijc.94143

Abstract: *This study aims to fabricate a $NiFe_2O_4/SiO_2/TiO_2$ magnetic composite to serve as a photocatalyst for the degradation of Congo red dye. The catalyst characterization involved XRD, FTIR, UV-vis DRS, BET, VSM, SEM-EDS, and pHpzc analyses. The performance in degradation was determined by the effect of various variables, including solution pH, dye concentration, and irradiation time. Results revealed that the $NiFe_2O_4/SiO_2/TiO_2$ composite exhibited a crystallite size of 24.56 nm and a bandgap of 2.1 eV. The surface area of $NiFe_2O_4/SiO_2/TiO_2$ was measured at 154 m^2/g, exceeding that of $NiFe_2O_4/SiO_2$ and $NiFe_2O_4$, which were observed at 122 and 51 m^2/g, respectively. $NiFe_2O_4/SiO_2/TiO_2$ exhibited magnetic properties with a magnetic saturation of 18.55 emu/g. Under optimal conditions (pH 5, initial dye concentration of 20 mg/L, and 90 min of visible irradiation), the degradation efficiency reached 96.86%. It was concluded that the photodegradation was effective, as its efficiency decreased from 96.86 to 92.45% after five reuse cycles. The presence of mineralization was evaluated using total organic carbon analysis, which revealed an 84.60% reduction in carbon content.*

Keywords: *$NiFe_2O_4/SiO_2/TiO_2$; magnetic composite; photodegradation; Congo red dye*

■ INTRODUCTION

Azo dyes, characterized by aromatic compounds linked via an azo-type chromophore group (−N=N−), are highly prevalent in industries like textiles, paper, printing, plastics, and leather [1-3]. Approximately 80% of these dyes are used in industries such as soap, paper, plastics, and textiles. During the synthesis and dyeing processes, about 10−15% of these dyes are released into water [4-5]. Their wastewater exhibits complex characteristics, including difficulty in degradation, and causes serious environmental damage once discharged without treatment [6-8]. Furthermore, dyestuffs are carcinogenic, mutagenic, stable to light and oxidizing agents, and difficult to remove from wastewater [6,9]. Congo red dye contains benzidine compounds, which are which are highly carcinogenic. Even at low concentrations and under specific temperatures, Congo red exhibits distinct color and toxicity. Its discharge into water not only jeopardizes human health but also disrupts plant photosynthesis. Furthermore, its azo structure makes it difficult to biodegradation. Therefore, effectively removing Congo red from industrial wastewater is crucial to safeguard human health and the ecological environment [10-11].

Various methods, such as adsorption [11], coagulation [12], electrochemical oxidation [13], biological treatment [14], and ion exchange [15] are applied to remove dyes from water. These methods only transfer contaminants from one phase to another, requiring additional processes, such as the advanced oxidation process [16]. Other drawbacks are the difficulty of reusing coagulants or flocculants, the high cost, and the recycling of adsorbents for sludge removal [17]. Advanced oxidation processes (AOP) are recognized as cost-effective, environmentally friendly, efficient, and promising approaches for decomposing and mineralizing pollutants [18-19]. Heterogeneous photocatalysis, a form of AOP, is a material capable of mineralizing numerous organic contaminants [20-22]. The dye is degraded after the semiconductor material is exposed to light. Photon absorption produces electron-hole pairs on the catalyst surface, reducing or oxidizing organic matter to non-toxic species, such as CO_2 and H_2O [20]. Some photocatalyst metal-semiconductors are TiO_2, ZnO, SnO_2, ZrO_2, V_2O_5, and C_3N_4, and several of their modifications have been studied [23-28].

TiO_2 is extensively employed due to its outstanding photocatalytic activity, chemical stability, non-toxic nature, affordability and low cost [22,29]. TiO_2 has excellent advantages, i.e., photosensitivity, chemical stability, and low cost [30]. TiO_2 is classified as n-type metal-oxide superconductors with a wide band gap [31]. Disadvantages of applying TiO_2 as a catalyst include a band gap of 3.2 eV, which limits absorption to UV light, and difficulty in separation from solution after the photocatalytic process, thereby causing the release of the material into the environment [32-33]. This problem can be solved by altering the structure of TiO_2, such as incorporating transition metals and doping with nonmetals, surface modification with organic compounds, and combining it with narrow bandgap semiconductors to generate heterojunctions [34-35].

Doping TiO_2 with magnetic materials is a method developed to enhance its photocatalytic activity while reducing band gap, photo dissolution, and recombination [32,35]. Combining this semiconductor with spinel ferrite results in a magnetic photocatalyst composite. Following the photodegradation process, the catalyst can be easily and quickly removed from the solution using permanent magnets. Spinel ferrite has the general formula MFe_2O_4, where M and Fe are metal cations located in two different places, tetrahedral and octahedral. One of the magnetic ferrites is $NiFe_2O_4$. The band gap energy of $NiFe_2O_4$ reported from the literature is around 2 eV [36-38]. Several modifications of TiO_2 include Fe_3O_4/TiO_2 to degrade methylene blue dye [30], $CoFe_2O_4/TiO_2$ to degrade Congo red dye [39], and $TiO_2/ZnFe_2O_4$ to degrade methylene blue dye [40].

$NiFe_2O_4$ is employed in electronic devices because of the chemical and mechanical stability, high permeability, electrical resistivity, and magnetic permeability [41-42]. Previous research has synthesized $NiFe_2O_4$ by co-precipitation, achieving a magnetic moment of 46.37 emu/g [43]. The modification of $NiFe_2O_4/TiO_2$ can reduce the band gap of TiO_2 from 3.20 to 2.11 eV, allowing $NiFe_2O_4/TiO_2$ to be used in the visible region. The reduction in the bandgap of semiconductor materials increases absorption wavelength, allowing electrons in the valence band to more easily transition to the conduction band [38]. A layer of SiO_2 between the $NiFe_2O_4$ and the TiO_2 shell is introduced to prevent electrons from being trapped by the magnetic core, which usually acts as a recombination for electron holes [44]. The recombination process reduces the efficiency of the photocatalytic. SiO_2 is the shell material due to its thermal stability, chemical inertness, and high specific surface area. In addition, SiO_2 protects $NiFe_2O_4$ from the agglomeration process [45]. The calcination temperature influences the characteristics of $NiFe_2O_4/SiO_2$. The crystallinity and magnetic properties of $NiFe_2O_4/SiO_2$ increase within the calcination range of 400–800 °C. At a calcination temperature of 800 °C, the crystal size of $NiFe_2O_4/SiO_2$ is 12.9 nm [46]. Previous research synthesized $NiFe_2O_4/SiO_2$ using the co-precipitation method with precursors $Ni(NO_3)_2 \cdot 6H_2O$ and $Fe(NO_3)_3 \cdot 9H_2O$ at a temperature of 450 °C, resulting in a crystallite size of 53.56 nm [43]. In this study, $NiFe_2O_4/SiO_2$ magnetic composites were synthesized using the co-precipitation method with precursors $NiCl_2 \cdot 6H_2O$ and $FeCl_3 \cdot 6H_2O$ at a calcination temperature of 800 °C, subsequently combined with TiO_2. These $NiFe_2O_4/SiO_2/TiO_2$ composites were employed to the photodegradation of Congo red dye.

■ EXPERIMENTAL SECTION

Materials

The materials used were $NiCl_2{\cdot}6H_2O$, $FeCl_3{\cdot}6H_2O$, NaOH, NH_4OH, tetraethyl orthosilicate (TEOS), HCl, titanium(IV) butoxide, TiO_2, ethanol, Congo red dye purchased from Merck (Germany), nitrogen gas, and deionized water.

Instrumentation

The X-ray diffractometer (XRD, Shimadzu-6000) was employed to determine the phase type and crystal size of the photocatalyst. Fourier transform infrared spectroscopy (FTIR, Prestige 21, Shimadzu) was applied to examine the functional groups. The elemental composition and morphology of the samples were evaluated by employing scanning electron microscopy with an energy dispersive spectrometer (SEM-EDS, Quanta-650 Oxford). UV-vis diffuse reflectance spectroscopy (UV-vis DRS, Pharmaspec, UV-1700) was used to analyze absorbance spectra. Surface area analysis was conducted using a Surface Area Analyzer (SAA, ASAP 2020). Magnetic properties were assessed using a Vibrating Sample Magnetometer (VSM Oxford Type 1.2 T). The concentration of Congo red dye was determined using a UV-vis spectrophotometer (Orion Aquamate 8000). Total organic carbon analysis was performed utilizing a Total Organic Carbon Analyzer (TOC Teledyne Tekmar).

Procedure

Synthesis of $NiFe_2O_4$

$NiFe_2O_4$ was synthesized using the co-precipitation method, a modification of the Naseri method [47]. Initially, 2.38 g of $NiCl_2{\cdot}6H_2O$ and 5.41 g of $FeCl_3{\cdot}6H_2O$ were dissolved in 40 mL of distilled water. After stirring the solution for 30 min, it was heated to 60 °C. A 2 M NaOH solution was gradually added while nitrogen gas was bubbled through the mixture to reach pH approximately 10. The $NiFe_2O_4$ precipitate was separated from the solution using an external magnet and then washed with ethanol and deionized water until the pH was neutral (pH 7). Finally, the product was dried in an oven at 70 °C for 1 h and then calcined in a furnace at 800 °C for 2 h.

Synthesis of $NiFe_2O_4/SiO_2$

Using a water bath sonicator, 1.0 g of $NiFe_2O_4$ was distributed throughout 50 mL of ethanol for 60 min at 25 °C. Furthermore, 10 mL of 25% NH_4OH was added, and the sonication process was continued for 15 min. After that, 8 mL of TEOS was added to the mixture, and the process was carried out for a further 2 h. The resulting precipitate was cleaned with ethanol and deionized water until it reached a pH of around 7. It was then dried in an oven for 1 h at 70 °C and calcined for 2 h at 800 °C in a furnace [46].

Synthesis of $NiFe_2O_4/SiO_2/TiO_2$

The source of TiO_2 in the synthesis of $NiFe_2O_4/SiO_2/TiO_2$ is titanium(IV) butoxide. To prepare the composite, 0.2 g of $NiFe_2O_4/SiO_2$ was added to 25 mL of ethanol over the course of 60 min at 25 °C in water bath sonicator. Subsequently, a solution of 0.1 M HCl was introduced to the mixture until the pH reached 4, and 0.2 mL of titanium(IV) butoxide (dissolved in 10 mL ethanol) was poured inside slowly and sonicated for 4 h. The residue obtained was washed using ethanol and deionized water to pH 7. Additionally, it was dried at 70 °C for 1 h and then calcined in a furnace at 800 °C for 2 h [47-48].

Determination of point of zero charge (pHpzc)

In each 100 mL conical flask, a 50 mL of 0.01 M NaCl solution was introduced. The initial pH of the solution was adjusted within the range of 2 to 12 by adding 0.1 M HCl or 0.1 M NaOH solution. Then, 0.2 g of $NiFe_2O_4/SiO_2/TiO_2$ magnetic composite was added to each flask, and the contents were agitated using a mechanical shaker for 48 h under atmospheric conditions. The pH at the point of zero charge was calculated by plotting the difference in pH (pH_{final}-$pH_{initial}$) against the initial difference in pH [49].

Photocatalytic activity

Congo red degradation using the $NiFe_2O_4/SiO_2/TiO_2$ magnetic composite was assessed using a reactor equipped with a visible light source (72 W LED lamps). The variables related to photocatalytic degradation comprised solution pH, dye concentration, and irradiation time. A 0.05 g of $NiFe_2O_4$-SiO_2-TiO_2 was mixed with 50 mL of 20 mg/L Congo red solution, and the pH of the solution was changed to range from 3 to 10 using 0.1 M HCl or NaOH. The mixture was put in the reactor and the position of the lamps with the reaction mixture was 25 cm from the visible lamp. The catalyst was isolated from the solution using a magnet, and the residual dye was examined. The effect of dye concentration was studied with variations of 20–120 mg/L (interval of 20 mg/L), while the irradiation time effect ranged from 0–120 min. The C/C_0 ratio, where C_0 and C are the dye concentrations prior to and following photodegradation, is used to express the degradation efficiency.

■ RESULTS AND DISCUSSION

XRD Analysis

Fig. 1 depicts the XRD spectra of $NiFe_2O_4$, $NiFe_2O_4/SiO_2$, and $NiFe_2O_4/SiO_2/TiO_2$. The peak of $NiFe_2O_4$ was observed to be sharp and intense at a value of 2θ, namely 30.37, 35.75, 43.43, 54.15, 57.41, 63.03, and 75.51°, according to the fields (220), (311), (400), (422), (511), (440) and (444). These data are consistent with the cubic spinel structure described in JCPDS Card No. 10-0325. The presence of peaks in the $NiFe_2O_4/SiO_2$ composite confirms that $NiFe_2O_4$ is the dominant phase. However, peaks indicative of SiO_2 were not observed, likely due to its amorphous properties [50-51]. The peaks corresponding to TiO_2 in the $NiFe_2O_4/SiO_2/TiO_2$ magnetic composite were detected at 25.53, 48.27, 55.35, and 71.51°, corresponding to the (101), (202), (105), and (116) crystallographic planes, respectively. These observations align with the data provided in JCPDS Card No. 21-1272, indicating the presence of the anatase phase in the composite material. The decrease in peak intensity observed in the magnetic composite suggests the successful coating of $NiFe_2O_4$ with SiO_2 and TiO_2. Table 1 presents the crystallite sizes of the three materials, calculated using Scherrer's formula. The coating process with SiO_2 and TiO_2 resulted in an increase in the crystallite size. These results are in line with earlier research by Kunarti et al. [51] and Han et al. [52], which found that Fe_3O_4 coated with SiO_2 and TiO_2 showed larger crystallites and lower peak intensity.

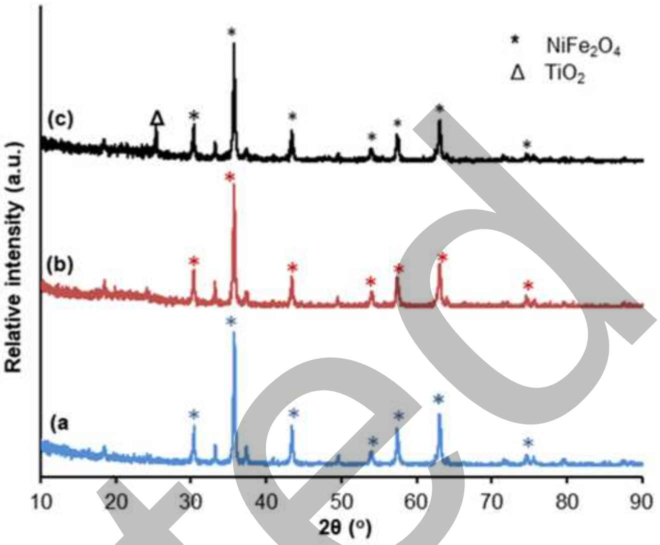

Fig 1. XRD diffraction pattern of (a) $NiFe_2O_4$, (b) $NiFe_2O_4/SiO_2$, and (c) $NiFe_2O_4/SiO_2/TiO_2$

Table 1. The crystallite size of the materials

Materials	Average crystallite size (nm)
$NiFe_2O_4$	18.88
$NiFe_2O_4/SiO_2$	20.73
$NiFe_2O_4/SiO_2/TiO_2$	24.56

FTIR Analysis

The functional groups of $NiFe_2O_4$, $NiFe_2O_4/SiO_2$, and $NiFe_2O_4/SiO_2/TiO_2$ were analyzed using FTIR, as shown in Fig. 2. The absorption at wavenumbers around 3200–3600 cm^{-1} indicated the presence of OH groups, derived from water molecules adsorbed by the catalyst and strengthened by a signal at 1600 cm^{-1} [53-54]. All three materials exhibit a similar absorption pattern at this specific wavenumber. The stretching vibrations of Ni–O and Fe–O were identified at 594 and 416 cm^{-1}, respectively, indicating the presence of the spinel structure of $NiFe_2O_4$. Furthermore, in the spectra of $NiFe_2O_4/SiO_2$ and $NiFe_2O_4/SiO_2/TiO_2$ at wavenumbers at 472, 796, and 1110 cm^{-1} signify the symmetric Si–O–Si stretching vibration [39,44]. The presence of TiO_2 was confirmed by absorption in the range of 400 to

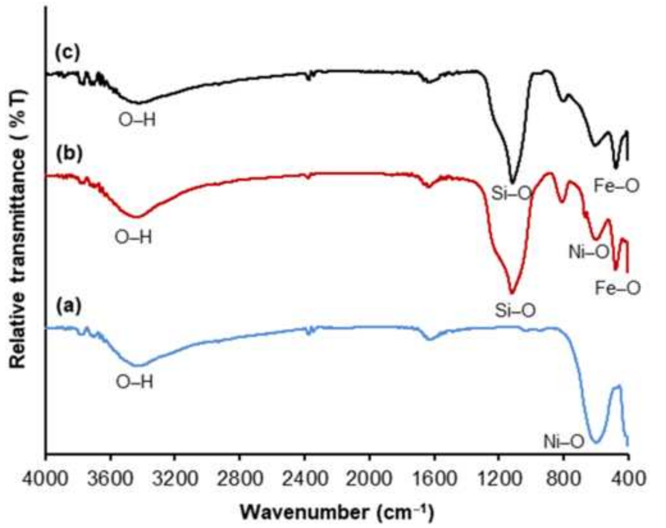

Fig 2. FTIR spectra of (a) $NiFe_2O_4$, (b) $NiFe_2O_4/SiO_2$, and (c) $NiFe_2O_4/SiO_2/TiO_2$

1000 cm^{-1}, with peaks at 470 and 788 cm^{-1} suggesting the contribution of Ti−O−Ti vibrations to TiO_2 (anatase) [53].

UV-vis DRS Analysis

The catalyst's optical characteristics were examined by UV-vis DRS analysis. Fig. 3(a) displays the UV-vis DRS spectrum of $NiFe_2O_4/SiO_2/TiO_2$ in comparison to commercial TiO_2. It was observed that TiO_2 was absorbed in the ultraviolet (355 nm) region and absent in the visible region, but the $NiFe_2O_4/SiO_2/TiO_2$ magnetic composites were absorbed both regions. Following Tauc's law, the bandgap energy value can be calculated from plot $(\alpha h\nu)^2$ versus energy (eV) as presented in Fig. 3(b). The bandgap energy value for TiO_2 and $NiFe_2O_4/SiO_2/TiO_2$ was 3.2 and 2.3 eV, respectively. The results suggest that the bandgap value of the composite decreased as a result of the core-shell structure.

BET Surface Area Analysis

According to Table 2, the surface areas of $NiFe_2O_4$, $NiFe_2O_4/SiO_2$, and $NiFe_2O_4/SiO_2/TiO_2$ were evaluated based on nitrogen gas absorption using the Brunauer-Emmett-Teller (BET) equation of 51, 122, and 154 m^2/g. Coating with SiO_2 and TiO_2 increased the surface area. Similarly, the other researchers found that the surface area of $CoFe_2O_4 < CoFe_2O_4/SiO_2 < CoFe_2O_4/SiO_2/TiO_2$ [55]. The pore diameter and pore volume of $NiFe_2O_4/SiO_2/TiO_2$ are 4.2 nm and 0.30 cm^3/g, indicating that this material is classified as mesopore (2–50 nm) [56]. The pore volume and diameter of $NiFe_2O_4/SiO_2/TiO_2$

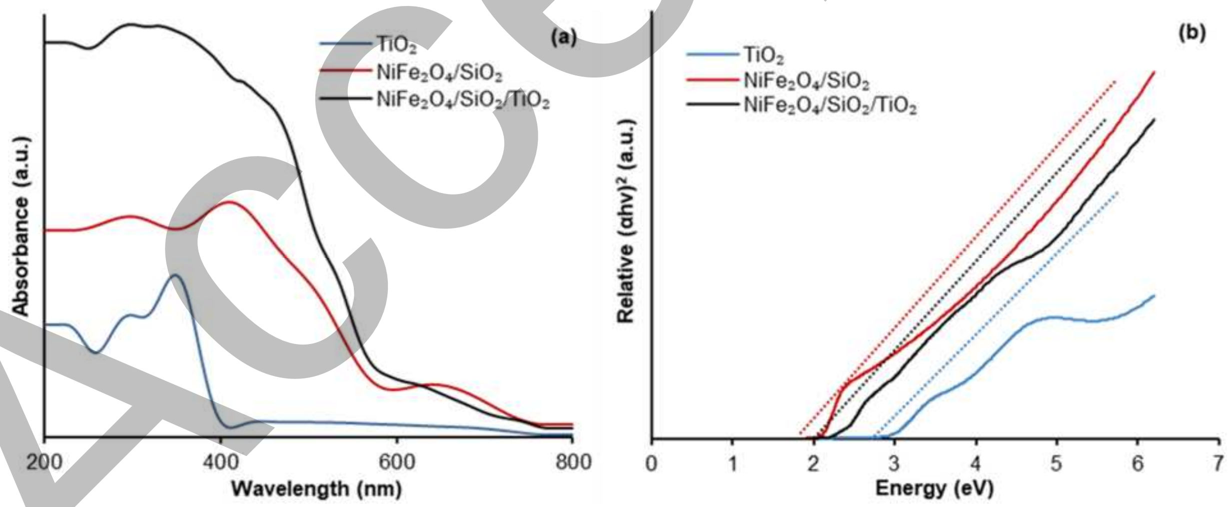

Fig 3. (a) UV-vis DRS, (b) plots $(\alpha h\nu)^2$ vs. E_g (eV) of the materials

Table 2. Parameters of the surface area of the materials

Materials	BET surface area (m^2/g)	d (nm)	V (cm^3/g)
$NiFe_2O_4$	51	3.8	0.24
$NiFe_2O_4/SiO_2$	122	3.7	0.24
$NiFe_2O_4/SiO_2/TiO_2$	154	4.2	0.30

are larger compared to $NiFe_2O_4$ and $NiFe_2O_4/SiO_2$, an increase in surface area can cause an increase in pore volume and diameter due to the addition of small pores or the creation of more spaces between the material particles.

VSM Analysis

Magnetic properties are an important aspect of magnetic photocatalysts. Fig. 4 shows the magnetic properties analysis of the materials. $NiFe_2O_4$ had the largest saturation magnetization of 43.48 emu/g, while $NiFe_2O_4/SiO_2$ and $NiFe_2O_4/SiO_2/TiO_2$ had 24.48 and 18.55 emu/g, respectively. Alavi et al. [57] reported the saturation magnetization of $NiFe_2O_4$ as 57.1 emu/g, but the formation of $NiFe_2O_4$-SiO_2-ZrO_2/SO_4^{2-}/Co/Cu magnetic composite decreased the value to 11.5 emu/g. Coating $NiFe_2O_4$ with $SrTiO_3$ reduced its saturation magnetization from 40 to 23.35 emu/g, according to another study [41]. Coating with non-magnetic materials often causes a reduction in magnetic properties. Despite the reduced properties observed, $NiFe_2O_4/SiO_2/TiO_2$ still exhibited good magnetic performance after being used in the photocatalytic process. Therefore, an external magnet can rapidly separate the catalyst from the solution.

SEM-EDS Analysis

Fig. 5 shows the morphology of the materials. The morphology of $NiFe_2O_4$ looks more homogeneous than that of other materials. $NiFe_2O_4/SiO_2$ morphology indicates the presence of spherical particles, which is characteristic of SiO_2 covering, while $NiFe_2O_4/SiO_2/TiO_2$ morphology has spherical particles with TiO_2 being suspected on the surface. SiO_2 addition as an interlayer between the $NiFe_2O_4$ core and the TiO_2 outer layer effectively reduced the interaction of $NiFe_2O_4$ and TiO_2 as well as protect the magnetic core from photo dissolution and electron-hole recombination [58]. Table 3 displays the composition of elements analyzed using EDS. The presence of Si and Ti in the magnetic composite confirmed the synthesis succeeded.

Photocatalytic Activity

In this research, the variables for photocatalytic degradation encompassed solution pH (3–10), dye concentration (20–120 mg/L), and irradiation time (0–120 min), as illustrated in Fig. 6. This figure depicts both the pHpzc and the influence of the three variables. In the photocatalytic degradation process, solution pH is a crucial factor that impacts the dye's charge. The determination of the pHpzc of $NiFe_2O_4/SiO_2/TiO_2$ was conducted at pH 6.5 to ascertain the total surface charge

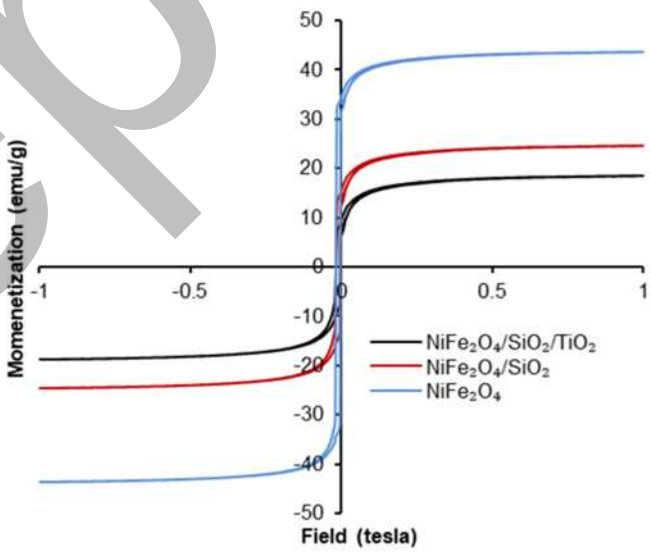

Fig 4. Magnetic hysteresis curve of the materials

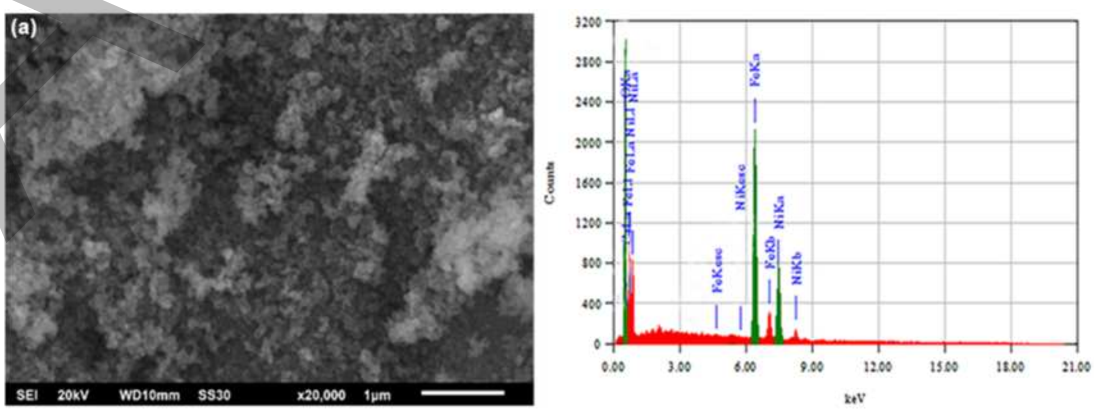

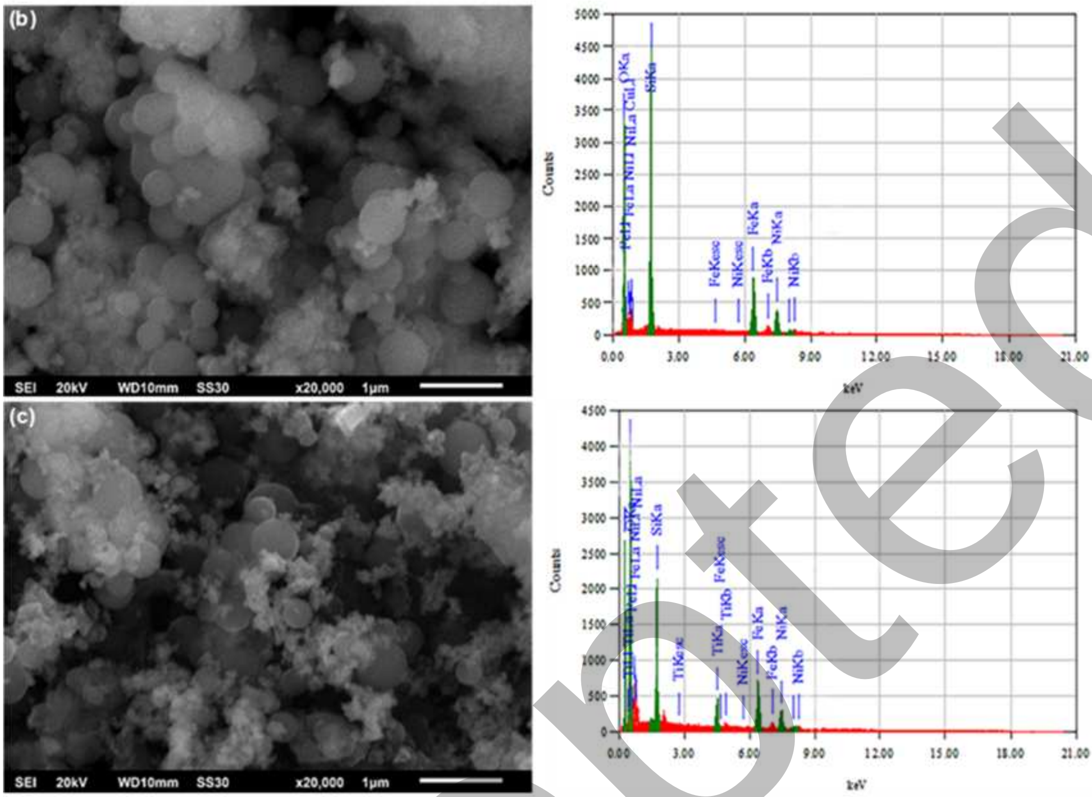

Fig 5. SEM image dan EDS spectra of (a) $NiFe_2O_4$, (b) $NiFe_2O_4/SiO_2$ and (c) $NiFe_2O_4/SiO_2/TiO_2$

Table 3. EDS analysis of the materials

Materials	Element (%)				
	O	Fe	Ni	Si	Ti
$NiFe_2O_4$	34.80	36.03	19.35	-	-
$NiFe_2O_4/SiO_2$	47.84	15.37	9.89	18.32	-
$NiFe_2O_4/SiO_2/TiO_2$	39.65	5.97	3.28	5.66	4.77

of the particles (Fig. 6(a)). If the solution has pH > pHpzc, then the composite surface is positively charged, but if the solution has pH < pHpzc, the charge of the composite surface becomes negative [44]. The catalyst and dye interaction is affected by the solution pH. Congo red dye has a pH range of 3.0–5.2, with pKa of 4.1. In acidic conditions (pH solution < pHpzc), it dissociates into negatively charged $R\text{-}SO_3^-$ from dye and interacts with the positively charged composite [50,58]. Electrostatic attraction is beneficial for dye adsorption on the catalyst surface, improving photodegradation performance [59]. Besides that, reducing O_2 to $\bullet O_2^-$ radical is expected to initiate under acidic conditions where the catalyst surface is positively charged by transferring electrons to the surface [60]. The pH effect on C/C_0 was determined by adding 0.05 g catalyst and 20 mg/L dye solution at a 60 min irradiation time (Fig. 6(b)). The highest degradation efficiency was observed at pH 5. In contrast, utilizing visible irradiation alone in the photolysis process did not yield significant changes.

An increase in dye concentration is directly related to a decrease in C/C_0 or inversely proportional to degradation efficiency. The dye obstructs visible irradiation from reaching the catalyst at higher concentrations, reducing efficiency [61]. Combining the catalyst with visible irradiation yielded higher degradation efficiency than using visible irradiation alone. A similar trend was observed in the degradation of etodolac with $ZnFe_2O_4/SiO_2/TiO_2$ composites, where UV irradiation alone resulted in lower degradation efficiency than when combined with a catalyst and UV irradiation. The effect of irradiation time was evaluated at 20 mg/L concentration of dye and a solution pH of 5. It was observed that the C/C_0 value decreased with increasing irradiation time up to 90 min, with an efficiency of 96.86%. Photocatalytic UV degradation of methylene blue using

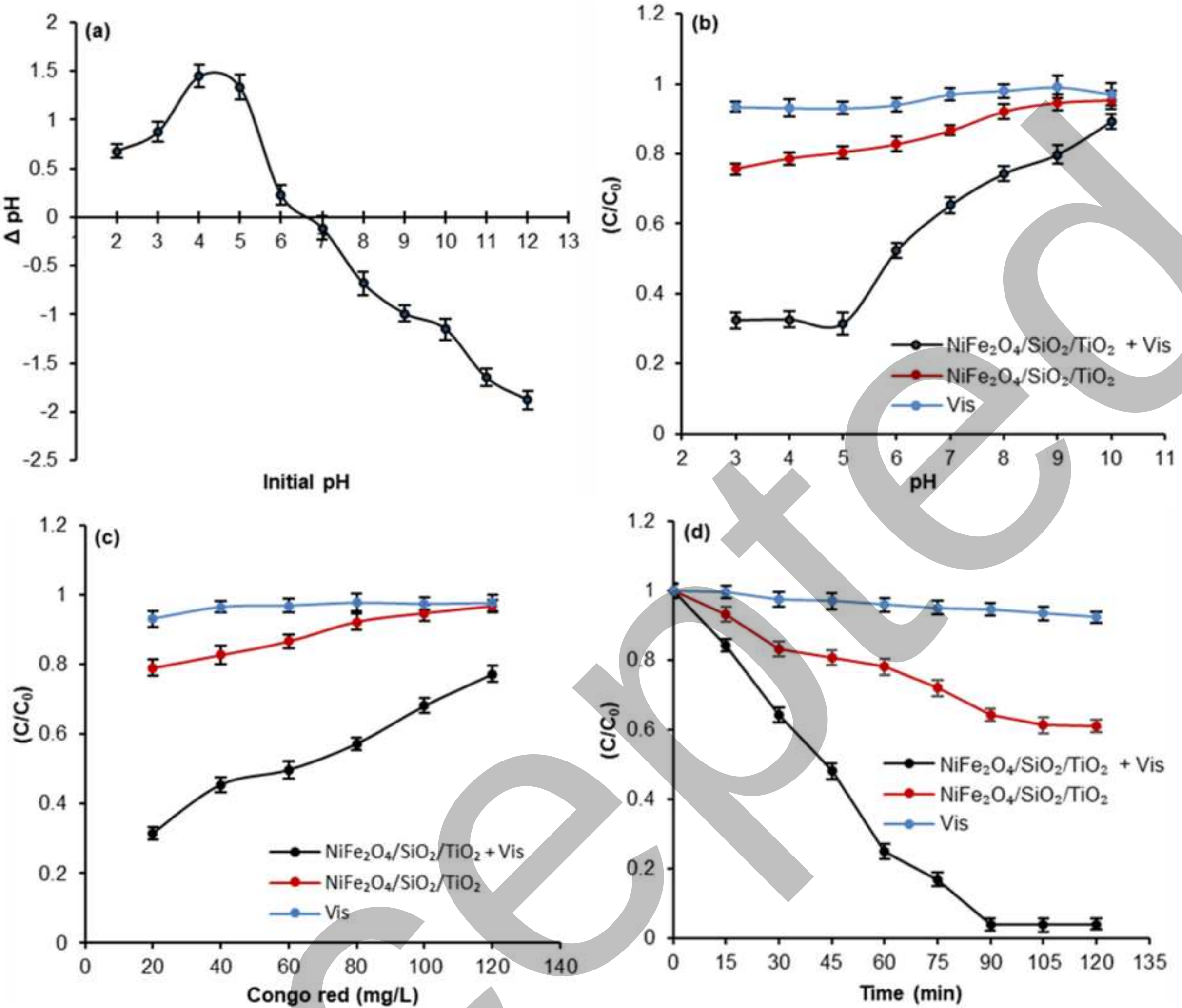

Fig 6. Photocatalytic degradation by varying (a) pHpzc, (b) solution pH, (c) Congo red dye concentration, and (d) irradiation time

$Fe_3O_4/SiO_2/TiO_2$ composites had the same pattern, which increased sharply at 0–120 min and continued slightly or remained relatively constant afterward [51]. In photocatalytic degradation, dye molecules are oxidized by reactive oxygen species produced, such as superoxide and hydroxyl radicals, on the surface of the catalyst, producing H_2O, CO_2, and other products [39]. Fig. 7 shows the schematic of the photodegradation of Congo red dye. The photocatalytic degradation utilizing $NiFe_2O_4/SiO_2/TiO_2$ composites can be explained in Eq. (1–8) [60-61];

$$NiFe_2O_4/SiO_4/TiO_2 + h\nu \rightarrow NiFe_2O_4/SiO_2/TiO_2(e^-_{CB} + h^+_{VB}) \quad (1)$$

$$h^+_{VB} + H_2O \rightarrow {}^{\bullet}OH^- + H^+ \quad (2)$$

$$e^-_{CB} + O_2 \rightarrow {}^{\bullet}O_2^- \quad (3)$$

$$^{\bullet}O_2^- + H_2O \rightarrow {}^{\bullet}HO_2 + OH^- \quad (4)$$

$$^{\bullet}O_2^- + H^+ \rightarrow {}^{\bullet}HO_2 \quad (5)$$

$$^{\bullet}HO_2 + H_2O \rightarrow H_2O_2 + {}^{\bullet}OH \quad (6)$$

$$H_2O_2 \rightarrow 2{}^{\bullet}OH \quad (7)$$

$$^{\bullet}H + {}^{\bullet}O_2^- + CR \rightarrow \text{Degradation product} \rightarrow CO_2 + H_2O + \text{other product} \quad (8)$$

Table 4 offers a comparison of the degradation efficiency of Congo red dye using various catalysts under varying pH, starting concentration, and irradiation time. The findings suggest that the $NiFe_2O_4/SiO_2/TiO_2$ composite exhibits potential for photodegradation compared to other catalysts.

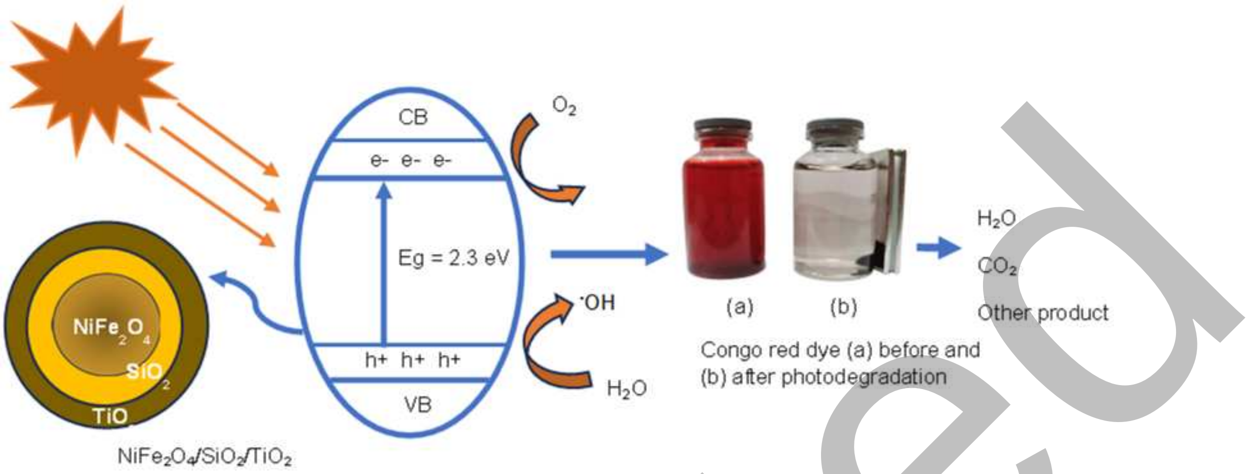

Fig 7. Schematic of photodegradation Congo red dye by $NiFe_2O_4/SiO_2/TiO_2$

Table 4. Comparison of Congo red degradation efficiency with previous reports catalyst

Catalyst	pH	Initial concentration (mg/L)	Irradiation time (min)	Degradations (%)	Ref.
$CoFe_2O_4$	9	10	90	92.00	[4]
$Co_3O_4/TiO_2/GO$	-	10	90	91.00	[62]
$g\text{-}C_3N_4/RGO/Bi_2Fe_4O_9$	-	10	60	87.65	[63]
$CTiO_2@Fe_3O_4/AC$	7	100	30	92.90	[64]
$Ni–TiO_2$	2	10	180	92.31	[65]
TiO_2	-	5	120	87.00	[66]
$P\text{-}ZrO_2CeO_2ZnO$	-	10	250	86.00	[67]
$NiFe_2O_4/SiO_2/TiO_2$	5	20	90	96.80	This work

Kinetic Study of Photodegradation

Degradation control mechanisms can be better understood with the use of kinetic models [30]. The pseudo-first-order rate model (as per the Langmuir-Hinshelwood model) allows one to ascertain the rate constant, k_{app}. Photodegradation reactions are typically described using this model, as shown in Eq. (9) and (10) [30,68];

$$r = \frac{dC}{dt} = -k_{app}C \tag{9}$$

$$\ln\frac{C_0}{C_t} = k_{app}t \tag{10}$$

where t is irradiation time, C_0 are C_t the initial concentrations and at the time of Congo red dye, k_{app} is obtained from the slope of $\ln\frac{C_0}{C_t}$ versus t plot. This study obtained a correlation coefficient (R^2) value of 0.983 before repeated and 0.929 after repeated. If the R^2 value was close to 1, proving the experimental data's suitability to the model used (Fig. 8). The k_{app} value obtained before and after it is repeated were 0.0376 and 0.0333 min^{-1}, respectively. The decrease in the k_{app} value can be attributed to the

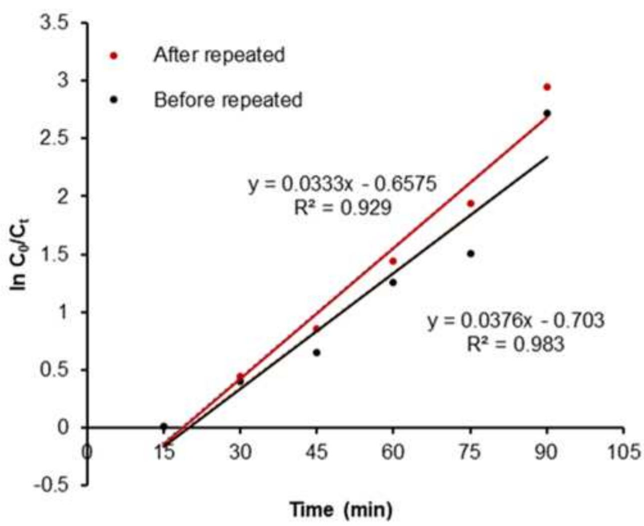

Fig 8. The kinetic curve for photodegradation of Congo red dye using $NiFe_2O_4/SiO_2/TiO_2$ before and after repeated

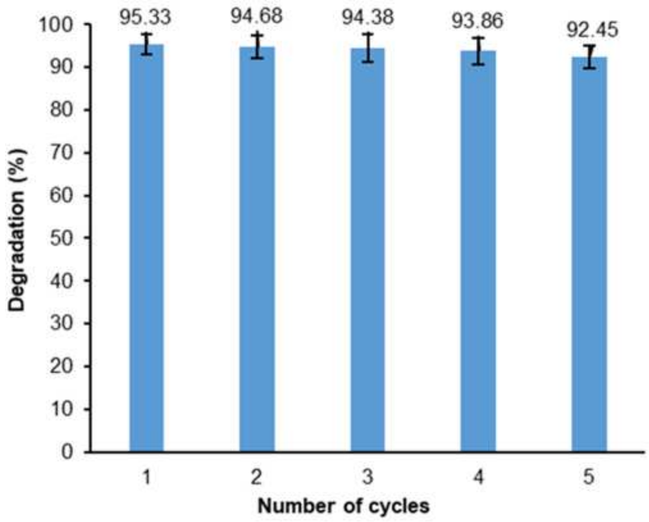

Fig 9. Reusability of $NiFe_2O_4/SiO_2/TiO_2$ for photocatalytic degradation

repeated use of the catalyst, which causes the dye to cover part of the catalyst surface.

Reusability of Composite

The catalyst's stability and reusability indicate that it can be used multiple times. Furthermore, the composite capability after five cycles is presented in Fig. 9. The initial Congo red concentration was 20 mg/L, the solution pH was 5, and the irradiation time was 90 min with a degradation efficiency of 96.86%. A catalyst that has already been used is cleaned with distilled water, dried, and then reused. After applying five cycles, the deterioration efficiency dropped from 96.86 to 92.45%. Compared to other research, namely using Fe_3O_4@Al_2O_3-PMo, the decreased efficiency 9.3% with five cycle experiments [61], this small decrease in the study demonstrates that $NiFe_2O_4/SiO_2/TiO_2$ is stable and highly efficient as the catalyst.

TOC analysis was conducted on the dye before and after photocatalytic degradation to assess the level of mineralization. The TOC value indicates the total organic compounds present in the solution [69]. This experiment utilized a Congo red dye concentration of 20 mg/L, a pH of 5, an irradiation time of 90 min, and a catalyst weight of 0.05 g. The efficiency of TOC reduction was 84.60%, indicating a successful decomposition process. This percentage is higher than 53.55% achieved using CeO_2/Ce-BiOBr [70] and 13.4% using carbon dots [69]. The decreased catalyst performance may be attributed to blocking active sites by dyes that remain on the catalyst during regeneration, hindering the diffusion of dye molecules to the catalyst's surface [71].

CONCLUSION

In this study, the $NiFe_2O_4/SiO_2/TiO_2$ composite has been successfully synthesized. The coating of $NiFe_2O_4$ with SiO_2 and TiO_2 resulted in reduced XRD diffractogram intensity and magnetic properties, alongside an increase in surface area. The composite demonstrates superparamagnetic properties, with a magnetic saturation value of 18.55 emu/g, a surface area of 154 m^2/g, and a bandgap value of 2.1 eV. The EDS results confirmed that the composite consisted of Ni, Fe, O, Si and Ti, which indicated that the synthesis was successful. It effectively catalyzed the photodegradation of Congo red dye. The degradation efficiency, with a concentration of 20 mg/L, pH of 5, and a visible irradiation for 90 min, was found to be 96.86%. The composite demonstrates high stability, enduring five cycles with only a minor decrease in efficiency (4.41%). Hence, it exhibits promise as a catalyst for wastewater treatment, particularly in scenarios involving dye-containing effluents. Outstanding magnetic properties play a pivotal role in photocatalysts as they facilitate easy recycling from solution by applying an external magnetic field.

ACKNOWLEDGMENTS

To conduct this research, the author is grateful to the Chemical Analysis and Instrumentation Laboratory, FMIPA, Universitas Sriwijaya.

CONFLICT OF INTEREST

The authors have no conflict of interest.

AUTHOR CONTRIBUTIONS

Poedji Loekitowati Hariani: conception and design of the research; conducting the investigation; writing and revising the manuscript. Salni: interpretation of data analysis and contributed to writing the manuscript. Nurlisa Hidayati: carried out the experiments and data characterization. Melviana Violetta Kimur: carried out the experiments and data analysis. Elfita: editing the manuscript and creating the visualizations. All authors reviewed and approved the final version of the manuscript.

REFERENCES

[1] Pang, X., Sellaoui, L., Franco, D., Dotto, G.L., Georgin, J., Bajahzar, A., Belmabrouk, H., Ben Lamine, A., Bonilla-Petriciolet, A., and Li, Z., 2019, Adsorption of crystal violet on biomasses from pecan nutshell, para chestnut husk, araucaria bark and palm cactus: Experimental study and theoretical modelling via monolayer and double layer statistical physics models, *Chem. Eng. J.*, 378, 122101.

[2] Li, Z., Sellaoui, L., Dotto, G.L., Lamine, A.B., Bonilla-Petriciolet, A., Hanafy, H., Belmabrouk, H., Netto, M.S., and Erto, A., 2019, Interpretation of the adsorption mechanism of Reactive Black 5 and Ponceau 4R dyes on chitosan/polyamide nanofibers via advanced statistical physics model, *J. Mol. Liq.*, 285, 165–170.

[3] Chen, F., Wu, X., Bu, R., and Yang, F., 2017, Co–Fe hydrotalcites for efficient removal of dye pollutants via synergistic adsorption and degradation, *RSC Adv.*, 7 (66), 41945–41954.

[4] Ali, N., Said, A., Ali, F., Razig, F., Ali, Z., Bilal, M., Reinert, L., Begum, T., and Igbal, H.M.N., 2020, Photocatalytic degradation of Congo red dye from aqueous environment using cobalt ferrite nanostructures: Development, characterization, and photocatalytic performance, *Water Air Soil Pollut.*, 231 (2), 50.

[5] Aziz, A., Ali, N., Khan, A., Bilal, M., Malik, S., Ali, N., and Khan, H., 2020, Chitosan-zinc sulfide nanoparticles, characterization and their photocatalytic degradation efficiency for azo dyes, *Int. J. Biol. Macromol.*, 153, 502–512.

[6] Zhou, Y., Ge, L., Fan, N., and Xia, M., 2018, Adsorption of Congo red from aqueous solution onto shrimp shell powder, *Adsorpt. Sci. Technol.*, 36 (5-6), 1310–1330.

[7] Khan, S., Khan, A., Ali, N., Ahmad., S., Ahmad, W., Malik, S., Ali, N., Shah, S., and Bilal, M., 2021, Degradation of Congo red dye using ternary metal selenide-chitosan microspheres as robust and reusable catalysts, *Environ. Technol. Innovation*, 22, 101402.

[8] Wagner, M., Eicheler, C., Helmreich, B., Hilbig, H., and Heinz, D., 2020, Removal of Congo red from aqueous solutions at hardened cement paste surfaces, *Front. Mater.*, 7, 567130.

[9] Yahya, N., Aziz, F., Jamaludin, N.A., Mutalib, M.A., Ismail, A.F., Salleh, W.N.W., Jaafar, J., Yusof, N., and Ludin, N.A., 2018, A review of integrated photocatalyst adsorbents for wastewater treatment, *J. Environ. Chem. Eng.*, 6 (6), 7411–7425.

[10] Li, Y., Meas, A., Shan, S., Yang, R., and Gai, X., 2016, Production and optimization of bamboo hydrochars for adsorption of Congo red and 2-naphthol, *Bioresour. Technol.*, 207, 379–386.

[11] Wang, R., Liu, Y., Lu, Y., Liang, S., Zhang, Y., Zhang, J., Shi, R., and Yin, W., 2023, Fabrication of a corn stalk derived cellulose-based bio-adsorbent to remove Congo red from wastewater: Investigation on its ultra-high adsorption performance and mechanism, *Int. J. Biol. Macromol.*, 241, 124545.

[12] Mcyotto, F., Wei, Q., Macharia, D.K., Huang, M., Shen, C., and Chow, C.W.K., 2021, Effect of dye structure on color removal efficiency by coagulation, *Chem. Eng. J.*, 405, 126674.

[13] Torres, N.H., Souza, B.S., Ferreira, L.F.R., Lima, A.S., dos Santos, G.N., and Cavalcanti, E.B., 2019, Real textile effluents treatment using coagulation/flocculation followed by electrochemical oxidation process and ecotoxicological assessment, *Chemosphere*, 236, 124309.

[14] Meerbergen, K., Willems, K.A., Dewil, R., Van Impe, J., and Lievens, B., 2018, Isolation and screening of bacterial isolates from wastewater treatment plants to decolorize azo dyes, *J. Biosci. Bioeng.*, 125 (4), 448–456.

[15] Fu, L., Shuang, C., Liu, F., Li, A., Li, Y., Zhou, Y., and Song, H., 2014, Shuang rapid removal of copper with magnetic poly-acrylic weak acid resin: Quantitative role of bead radius on ion exchange, *J. Hazard. Mater.*, 272, 102–111.

[16] Argote-Fuentes, S., Feria-Reyes, R., Ramos-Ramírez, E., Gutiérrez-Ortega, N., and Cruz-Jiménez, G., 2021, Photoelectrocatalytic degradation of Congo red dye with activated hydrotalcites and copper anode, *Catalysts*, 11 (2), 211.

[17] Sohni, S., Gul, K., Ahmad, F., Ahmad, I., Khan, A., Khan, N., and Bahadar Khan, S., 2018, Highly efficient removal of Acid red-17 and Bromophenol blue dyes from industrial wastewater using graphene oxide functionalized magnetic chitosan composite, *Polym. Compos.*, 39 (9), 3317–3328.

[18] Benamira, M., Lahmar, H., Messaadia, L., Rekhila, G., Akika, F.Z., Himrane, M., and Trari, M., 2020, Hydrogen production on the new hetero-system Pr_2NiO_4/SnO_2 under visible light irradiation, *Int. J. Hydrogen Energy*, 45 (3), 1719–1728.

[19] Lahmar, H., Benamira, M., Douafer, S., Akika, F.Z., Hamdi, M., Avramova, I., and Trari, M., 2020, Photocatalytic degradation of crystal violet dye on the novel $CuCr_2O_4/SnO_2$ hetero-system under sunlight, *Optik*, 219, 165042.

[20] Motahari, F., Mozdianfard, M.R., Soofivand, F., and Salavati-Niasari, M., 2014, NiO nanostructures: Synthesis, characterization and photocatalyst application in dye wastewater treatment, *RSC Adv.*, 4 (53), 27654–27660.

[21] Wang, Y.S., Shen, J.H., and Horng, J.J., 2014, Chromate enhanced visible light driven TiO_2 photocatalytic mechanism on Acid Orange 7 photodegradation, *J. Hazard. Mater.*, 274, 420–427.

[22] Starukh, G., 2017, Photocatalytically enhanced cationic dye removal with Zn-Al layered double hydroxides, *Nanoscale Res. Lett.*, 12 (1), 391.

[23] Janczarek, M., and Kowalska, E., 2017, On the origin of enhanced photocatalytic activity of copper-modified titania in the oxidative reaction systems, *Catalysts*, 7 (11), 317.

[24] Zhong, Z., Etim, U.J., and Song, Y., 2020, Improving the Cu/ZnO-based catalysts for carbon dioxide hydrogenation to methanol, and the use of methanol as a renewable energy storage media, *Front. Energy Res.*, 8, 545431.

[25] Bejtka, K., Zeng, J., Sacco, A., Castellino, M., Hernández, S., Farkhondehfal, M.A., Savino, U., Ansaloni, S., Pirri, C.F., and Chiodoni, A., 2019, Chainlike mesoporous SnO_2 as a well-performing catalyst for electrochemical CO_2 reduction, *ACS Appl. Energy Mater.*, 2 (5), 3081–3091.

[26] Zhuang, H., Bai, S., Liu, X., and Yan, Z., 2010, Structure and performance of Cu/ZrO_2 catalyst for the synthesis of methanol from CO_2 hydrogenation, *J. Fuel Chem. Technol.*, 38 (4), 462–467.

[27] Gurram, V.R.B., Enumula, S.S., Mutyala, S., Pocharmoni, R., Prasad, P.S.S., Burri, D.R., and Kamraju, S.R.R., 2016, The advantage of ceria loading over V_2O_5/Al_2O_3 catalyst for vapor phase oxidative dehydrogenation of ethylbenzene to styrene using CO_2 as a soft oxidant, *Appl. Petrochem. Res.*, 6 (4), 427–437.

[28] Pattnaik, S.P., Behera, A., Acharya, R., and Parida, K., 2019, Green exfoliation of graphitic carbon nitride towards decolourization of Congo-red under solar irradiation, *J. Environ. Chem. Eng.*, 7 (6), 103456.

[29] Moreira, N.F.F., Sousa, J.M., Macedo, G., Ribeiro, A.R., Barreiros, L., Pedrosa, M., Faria, J.L., Pereira, M.F.R., Castro-Silva, S., Segundo, M.A., Manaia, C.M., Nunes, O.C., and Silva, A.M.T., 2016, Photocatalytic ozonation of urban wastewater and surface water using immobilized TiO_2 with LEDs: Micropollutants, antibiotic resistance genes and estrogenic activity, *Water Res.*, 94, 10–22.

[30] Tumbelaka, R.M., Istiqomah, N.I., Kato, T., Oshima, D., and Suharyadi, E., 2022, High reusability of green-synthesized Fe_3O_4/TiO_2 photocatalyst nanoparticles for efficient degradation of methylene blue dye, *Mater. Today Commun.*, 33, 104450.

[31] Shayegan, Z., Lee, C.S., and Haghighat, F., 2018, TiO_2 photocatalyst for removal of volatile organic compounds in gas phase – A review, *Chem. Eng. J.*, 334, 2408–2439.

[32] Gebrezgiabher, M., Gebreslassie, G., Gebretsadik, T., Yeabyo, G., Elemo, F., Bayeh, Y., Thomas, M., and Linert, W., 2019, A C-doped TiO_2/Fe_3O_4 nanocomposite for photocatalytic dye degradation

under natural sunlight irradiation, *J. Compos. Sci.*, 3 (3), 75.

[33] Gabelica, I., Ćurković, L., Mandić, V., Panžić, I., Ljubas, D., and Zadro, K., 2021, Rapid microwave-assisted synthesis of $Fe_3O_4/SiO_2/TiO_2$ core-2-layer-shell nanocomposite for photocatalytic degradation of ciprofloxacin, *Catalysts*, 11 (10), 1136.

[34] Zhang, Y., Shi, Z., Luo, L., Liu, Z., Macharia, D.K., Duoerkun, G., Shen, C., Liu, J., and Zhang, L., 2020, Construction of titanium dioxide/cadmium sulfide heterojunction on carbon fibers as weavable photocatalyst for eliminating various contaminants, *J. Colloid Interface Sci.*, 561, 307–317.

[35] Boulahbel, H., Benamira, M., Bouremmad, F., Ahmia, N., Kiamouche, S., Lahmar, H., Souici, A., and Trari, M., 2023, Enhanced photodegradation of Congo red dye under sunlight irradiation by p-n $NiFe_2O_4/TiO_2$ heterostructure, *Inorg. Chem. Commun.*, 154, 110921.

[36] Hariani, P.L., Said, M., Rachmat, A., Riyanti, F., Pratiwi, H.C., and Rizki, W.T., 2022, Preparation of $NiFe_2O_4$ nanoparticles by solution combustion method as photocatalyst of Congo red, *Bull. Chem. React. Eng. Catal.*, 16 (3), 481–490.

[37] Verdi, I.R., Maroli Neto, A.J., Garcia, I.S.G., Lenzi, G.G., Villetti, M.A., Alves, O.C., Fidelis, M.Z., da Rocha, R.D.C., and Brackmann, R., 2024, Magnetic $NiFe_2O_4/TiO_2$ heterostructures for the photocatalytic decontamination of glyphosate in water, *Mater. Sci. Semicond. Process.*, 174, 108205.

[38] Wang, W., Zhang, L., Liu, Z., Kang, L., Chen, Q., Wang, W., Liu, M., Ye, B.C., Yu, F., and Li, Y., 2022, Visible-light-activated TiO_2–$NiFe_2O_4$ heterojunction for detecting sub-ppm trimethylamine, *J. Alloys Compd.*, 898, 162990.

[39] Magdalane, C.M., Priyadharsini, G.M.A., Kaviyarasu, K., Jothi, A.I., and Simiyon, G.G., 2021, Synthesis and characterization of TiO_2 doped cobalt ferrite nanoparticles via microwave method: Investigation of photocatalytic performance of Congo red degradation dye, *Surf. Interfaces*, 25, 101296.

[40] Coromelci, C., Neamtu, M., Ignat, M., Samoila, P., Zaltariov, M.F., and Palamaru, M., 2022, Ultrasound assisted synthesis of heterostructured $TiO_2/ZnFe_2O_4$ and $TiO_2/ZnFe_{1.98}La_{002}O_4$ systems as tunable photocatalysts for efficient organic pollutants removal, *Ceram. Int.*, 48 (4), 4829–4840.

[41] Xia, Y., He, Z., Lu, Y., Tang, B., Sun, S., Su, J., and Li, X., 2018, Fabrication and photocatalytic property of magnetic $SrTiO_3/NiFe_2O_4$ heterojunction nanocomposites, *RSC. Adv.*, 8 (10), 5441–5450.

[42] Sivakumar, P., Ramesh, R., Ramanand, A., Ponnusamy, S., and Muthamizhchelvan, C., 2013, Synthesis and characterization of $NiFe_2O_4$ nanoparticles and nanorods, *J. Alloys Compd.*, 563, 6–11.

[43] Hariani, P.L., Said, M., Rachmat, A., Salni, S., Aprianti, N., and Amatullah, A.F., 2022, Synthesis of $NiFe_2O_4/SiO_2/NiO$ magnetic and application for the photocatalytic degradation of Methyl orange dye under UV irradiation, *Bull. Chem. React. Eng. Catal.*, 17 (4), 699–711.

[44] Alwared, A.I., Sulaiman, F.A., Raad, H., Al-Musawi, T.J., and Mohammed, N.A., 2023, Ability of $FeNi_3/SiO_2/TiO_2$ nanocomposite to degrade amoxicillin in wastewater samples in solar light-driven processes, *S. Afr. J. Bot.*, 153, 195–202.

[45] Yulizar, Y., Apriandanu, D.O.B., and Zahra, Z.A., 2021, $SiO_2/NiFe_2O_4$ nanocomposites: Synthesis, characterization and their catalytic activity for 4-nitroaniline reduction, *Mater. Chem. Phys.*, 261, 124243.

[46] Czempik, A., Grasset, F., Auguste, S., Rousseau, A., Kubacki, J., Sobol, T., Szczepanik, M., Randrianantoandro, N., and Bajorek, A., 2024, Unraveling the effect of annealing on the structural and microstructural evolution of $NiFe_2O_4@SiO_2$ core-shell type nanocomposites, *Ceram. Int.*, 50 (11, Part B), 20473–20494.

[47] Naseri, A., Goodarzi, M., and Ghanbari, D., 2017, Green synthesis and characterization of magnetic and effective photocatalyst $NiFe_2O_4$–NiO

nanocomposites, *J. Mater. Sci.: Mater. Electron.*, 28 (23), 17635–17646.

[48] Castro-Beltrán, A., Luque, P.A., Garrafa-Gálvez, H.E., Vargas-Ortiz, R.A., Hurtado-Macías, A., Olivas, A., Almaral-Sánchez, J.L., and Alvarado-Beltrán, C.G., 2018, Titanium butoxide molar ratio effect in the TiO_2 nanoparticles size and Methylene blue degradation, *Optik*, 157, 890–894.

[49] Kumar, D., and Gupta, S.K., 2023, Green synthesis of novel biochar from *Abelmoschus esculentus* seeds for direct blue 86 dye removal: Characterization, RSM optimization, isotherms, kinetics, and fixed bed column studies, *Environ. Pollut.*, 337, 122559.

[50] Hariani, P.L., Said, M., Salni, S., Aprianti, N., and Naibaho, Y.A.L.R., 2022, High efficient photocatalytic degradation of Methyl orange dye in an aqueous solution by $CoFe_2O_4$-SiO_2-TiO_2 magnetic catalyst, *J. Ecol. Eng.*, 23 (1), 118–128.

[51] Kunarti, E.S., Roto, R., Pradipta, A.R., and Budi, I.S., 2017, $Fe_3O_4/SiO_2/TiO_2$ core-shell nanoparticles as catalyst for photoreduction of Ag(I) ions, *Orient. J. Chem.*, 33 (4), 1933–1940.

[52] Han, K.H., Kim, Y.H., Pak, I.H., Yu, J.H., Ho, I.C., and Han, R.H., 2022, Fe_3O_4@SiO_2@TiO_2@PDA nanocomposite for the degradation of organic materials, *Chem. Eng. Technol.*, 45 (1), 178–188.

[53] Praveen, P., Viruthagiri, G., Mugundan, S., and Shanmugam, N., 2014, Structural, optical and morphological analyses of pristine titanium di-oxide nanoparticles – Synthesized via sol–gel route, *Spectrochim. Acta, Part A*, 117, 622–629.

[54] Cathrin Lims, S., Divya, S., and Jose, M., 2023, Design of CuO@SiO_2 core shell nanocomposites and its applications to photocatalytic degradation of Rhodamine B dye, *Opt. Mater.*, 144, 114356.

[55] Zielińska-Jurek, A., Bielan, Z., Dudziak, S., Wolak, I., Sobczak, Z., Klimczuk, T., Nowaczyk, G., and Hupka, J., 2017, Design and application of magnetic photocatalysts for water treatment. The effect of particle charge on surface functionality, *Catalyst*, 7 (12), 360.

[56] Chand, K., Jiao, C., Lakhan, M.N., Shah, A.H., Kumar, V., Fouad, D.E., Chandio, M.B., Ali Maitlo, A., Ahmed, M., and Cao, D., 2021, Green synthesis, characterization and photocatalytic activity of silver nanoparticles synthesized with *Nigella sativa* seed extract, *Chem. Phys. Lett.*, 763, 138218.

[57] Alavi, S.A., Nasseri, M.A., Kazemnejadi, M., Allahresani, A., and HussainZadeh, M., 2021, $NiFe_2O_4$@SiO_2@ZrO_2/SO_4^{2-}/Cu/Co nanoparticles: a novel, efficient, magnetically recyclable and bimetallic catalyst for Pd-free Suzuki, Heck and C–N cross-coupling reactions in aqueous media, *New J. Chem.*, 45 (17), 7741–7751.

[58] Lafi, R., Montasser, I., and Hafiane, A., 2018, Adsorption of Congo red dye from aqueous solutions by prepared activated carbon with oxygen-containing functional groups and its regeneration, *Adsorp. Sci. Technol.*, 37 (1-2), 160–181.

[59] Li, Y., Li, J., Pan, Y., Xiong, Z., Yao, G., Xie, R., and Lai, B., 2020, Peroxymonosulfate activation on $FeCo_2S_4$ modified g-C_3N_4 ($FeCo_2S_4$-CN): Mechanism of singlet oxygen evolution for nonradical efficient degradation of sulfamethoxazole, *Chem. Eng. J.*, 384, 123361.

[60] Adeel, M., Saeed, M., Khan, I., Muneer, M., and Akram, N., 2021, Synthesis and characterization of Co–ZnO and evaluation of its photocatalytic activity for photodegradation of methyl orange, *ACS Omega*, 6 (2), 1426–1435.

[61] Ammar, S.H., Ibrahim Elaibi, A., and Sh. Mohammed, I., 2020, Core/shell Fe_3O_4@Al_2O_3-PMo magnetic nanocatalyst for photocatalytic degradation of organic pollutants in an internal loop airlift reactor, *J. Water Process Eng.*, 37, 101240.

[62] Jo, W.K., Kumar, S., Isaacs, M.A., Lee, A.F., and Karthikeyan, S., 2017, Cobalt promoted TiO_2/GO for the photocatalytic degradation of oxytetracycline and Congo red, *Appl. Catal., B*, 201, 159–168.

[63] Shekardasht, M.B., Givianrad, M.H., Gharbani, P., Mirjafary, Z., and Mehrizad, A., 2020, Preparation of a novel Z-scheme g-C_3N_4/RGO/$Bi_2Fe_4O_9$ nanophotocatalyst for degradation of Congo red

dye under visible light, *Diamond Relat. Mater.*, 109, 108008.

[64] Zhu, L., Kong, X., Yang, C., Ren, B., and Tang, Q., 2020, Fabrication and characterization of the magnetic separation photocatalyst $CTiO_2@Fe_3O_4/AC$ with enhanced photocatalytic performance under visible light irradiation, *J. Hazard. Mater.*, 381, 120910.

[65] Indira, K., Shanmugam, S., Hari, A., Vasantharaj, S., Sathiyavimal, S., Brindhadevi, K., El Askary, A., Elfasakhany, A., and Pugazhendhi, A., 2021, Photocatalytic degradation of Congo red dye using nickel–titanium dioxide nanoflakes synthesized by *Mukia madrasapatna* leaf extract, *Environ. Res.*, 202, 111647.

[66] Langa, C., Tetana, Z.N., and Hinstsho-Mbita, N.C., 2023, Effect of calcination temperature on the synthesis of TiO_2 nanoparticles from *Sutherlandia frutescence* for the degradation of Congo red dye and antibiotics ciproflaxin and sulfamethoxazole, *Chem. Phys. Impact*, 7, 100389.

[67] Hokonya, N., Mahamadi, C., Mukaratirwa-Muchanyereyi, N., Gutu, T., and Zvinowanda, C., 2022, Green synthesis of $P\text{-}ZrO_2CeO_2ZnO$ nanoparticles using leaf extracts of *Flacourtia indica* and their application for the photocatalytic degradation of a model toxic dye, Congo red, *Heliyon*, 8 (8), e10277.

[68] Dash, L., Biswas, R., Ghost, R., Kaur, V., Banerjee, B., Sen, T., Patil, R.A., Ma, Y.R., and Haldar, K.K., 2020, Fabrication of mesoporous titanium dioxide using *Azadirachta indica* leaves extract towards visible-light-driven photocatalytic dye degradation, *J. Photochem. Photobiol., A*, 400, 112682.

[69] Abassi, A., Abushad, M., Khan, A., Bhat, Z.U.H., Hanif, S., and Shakir, M., 2023, Bare undoped nontoxic carbon dots as a visible light photocatalyst for the degradation of methylene blue and Congo red, *Carbon Trends*, 10, 100238.

[70] Chen, D., Xu, X., Lei, P., Ge, J., Tong, Y., Huang, C., and Fu, X., 2023, One-pot solvothermal assembly of CeO_2/Ce-BiOBr hollow microsphere heterojunctions for efficient degradation of Congo red driven by visible LED light irradiation, *Colloids Surf., A*, 672, 131751.

[71] Ichipi, E.O., Mapossa, A.B., Costa, A.C.F.M., Chirwa, E.M.N., and Tichapondwa, S.M., 2023, Fabrication and characterization of recyclable, magnetic $(CoFe_2O_4)_x/Ag_2S\text{-}ZnO$ composites for visible-light-induced photocatalytic degradation of methylene blue dye, *J. Water Process Eng.*, 54, 104040.